IEEE Access
Multidisciplinary | Rapid Review | Open Access Journal

Received December 23, 2021, accepted January 10, 2022, date of publication January 26, 2022, date of current version February 11, 2022.

Digital Object Identifier 10.1109/ACCESS.2022.3146392

Design of Robust Guaranteed Margin Stability Region PI Controller for Automotive LED Lighting With Parameter Uncertainty

ALAGARSAMY SURESHKUMAR AND RAMACHANDIRAN GUNABALAN, (Member, IEEE)
School of Electrical Engineering, Vellore Institute of Technology, Chennai, Tamil Nadu 600127, India
Corresponding author: Ramachandiran Gunabalan (gunabalan.r@vit.ac.in)

ABSTRACT In the modern era, automotive light emitting diode (LED) lighting technologies are booming as a result of high luminous intensity, long life, compact size, high energy efficiency, high reliability etc. As the load is sensitive for input parametric variations, it is essential to regulate the load voltage and current with respect to system specifications. Hence, there is a need for fast response robust controller to feed the required voltage and current during abnormal conditions. In this paper, a robust controller is designed for single switch control buck boost converter for automotive LED lighting. A small signal modelling of the converter is developed with perturbed state variables to analyze the dynamic behavior of the system. The system with dynamic controller has a zero in the right-hand side of the s-plane, which results in poor closed loop stability. Hence, a robust controller is designed with Kharitonov's theorem by considering the uncertain variations in the converter parameters. A robust performance region is obtained by considering guaranteed gain margin and phase margin benchmark. In this region, the optimal PI controller gain values are obtained using Kharitonov's sixteen plants theorem. The obtained gain values make the system with minimum oscillation, fast settling time, right hand side zero compensation and stability of the system. The performance analysis is compared with the conventional PI controller and to ensure the peak value of sensitivity for robust controller. The simulation of the system is performed in PSIM and validated in real time using dSPACE1103 controller with experimental results.

INDEX TERMS DC–DC power converter, Kharitonov's theorem, LED lamps, robust control, stability, uncertain systems.

I. INTRODUCTION

Lighting technology has significant role in indoor and outdoor lightings, automotive applications etc. In recent days, fluorescent and incandescent lamps are being replaced by LED lamps by its advantages like high luminous efficiency, dimming control, high reliability, small size, robustness and color rendering index [1]. In the automotive LED lighting applications, exterior lights were used as head lights, fog lights, stop/tail lights and turn indicators. LED front light could provide high brightness and less heat dissipation when compared with traditional halogen and xenon lamp in vehicles [2]. Recently, LED lighting is used in environmental friendly electric vehicles in which power is supplied from a battery. In recent years, 48 V battery is used in BLDC motor controller, telecommunication equipment and mild hybrid electric vehicles [3]. Automotive mild EV system uses 48 V battery and the voltage varies between 52 V to 38 V during driving period and voltage dips to 28 V during cold crank. Also, voltage varies dynamically during sudden stop and unclamped load dump condition [4]. The voltage and current variations damage the LED driver when exceeds nominal values. Hence, an efficient converter with appropriate closed loop controller is required to regulate the load voltage by maintaining constant current.

The converter selection plays a vital role for LED driver applications. A DC-DC converter is operated in buck [5], boost [6] and buck-boost (BB) modes of operation based on the available input voltage. For automotive lighting applications, BB converter is generally preferred because of wide range of variations in input voltage. BB converters were investigated for automotive applications with 12 V [7], 24 V [8] and 48 V [9]. Yaxiao Q developed a four-switch noninverting BB converter with 96% maximum efficiency.

The associate editor coordinating the review of this manuscript and approving it for publication was Zhe Zhang.

Though, the system has higher efficiency, the voltage gain of the converter is less than unity [8]. A two-stage resonant BB LED driver was developed in [7] and full bridge series resonant converter was proposed in [9]. In those topologies, efficiency is maintained constant (93%) for wide range of input variations. In [10], a single switch-controlled LED driver with parasitic model with minimum phase system was developed. The efficiency of the converter was maintained between 91% and 95% for wide input variations with less number of active and passive components. In addition, stability of the system was investigated with derived open loop model of the converter. There exists a zero in the right half of s- plane (RHP) for duty cycle to output voltage transfer function which results in stability issue [11]. To overcome this, a compensator was introduced in the system using current/ voltage mode controllers. In [12], a current mode control (CMC) was used in DC-DC converter to compensate the RHP zeros. It results in instability issues when the converter was operated with duty cycle greater than 0.5. In addition, sub harmonics oscillation occurs with poor load regulation. It is not preferred for low power applications. Voltage mode control (VMC) is preferred for the system which requires wide range of duty cycle control with dynamic variations.

In [13], modified diode-capacitor DC-DC converter with PI controller for regulating the output voltage was developed. The control scheme results in good dynamic response for high voltage applications and poor response for low voltage applications. This problem was overcome using causal path of bond graph method [14]. The detailed design guidelines for eliminating RHP zero were specified by identifying the polarity of zeros of the causal path. The transfer function was obtained by considering the feed forward path which results is computational problem for the system with more number of forward paths. Tri state BB converter with PI and type 3 partial swam optimization was proposed [15]. The controller was implemented using analog components, but the efficiency of the system was reduced when compared with conventional BB converter with non-minimal phase problem. This issue was addressed in [16], with robust PID controller. The proposed controller reduces the complex tuning effect of the controller parameters and allows the converter to operate close to the performance limit with zero in RHP. Zhang and Guo [17] investigated the second order non-linear uncertain dynamical system and pointed out the importance of PID tuning. In [18], a modern PI(D) controller was developed for parameter variations using Kharitonov's theorem. It was used for robust controller design for possible system plant variations, right hand side zero (RHZ) compensation and guaranteed margin performance.

The open loop system of a single switch modified H bridge converter (MHBC) was investigated for wide range of input variations [10]. The closed loop stability of the system was investigated with loop model. As an extension, in this work, a controller is designed for wide range of input variations and parameter variations. These variations are uncertain in nature which is called as structure uncertainty, which requires a robust controller. In the suggested work, a robust controller is designed for parametric uncertainty model of the converter. The interval plant stability analysis and controller gain regions using Kharitonov's theorem under guaranteed gain and phase margin were carried out. Sixteen Kharitonv's plants theorem is used to find the common controller gain region in all possible plant uncertainty. The controller gain values for this area are evaluated in terms of time domain specifications, pole zero mapping and sensitivity. The performance analysis was compared with conventional PI controller design by using MATLAB – SISO software tool.

Organization of this paper is as follows: Section II explains the steady state and small signal modeling of MHBC. Section III explains the robust controller design including performance analysis of the controller gain, and Section IV explains the simulation and experimental results. The conclusion is summarized in section V.

II. STEADY STATE AND SMALL SIGNAL MODELLING OF MHBC

A. CIRCUIT DESCRIPTION

Fig. 1 shows the circuit diagram of a MHBC, in which switch S_1 is triggered with fixed duty cycle and switch S_2 is controlled by robust PI controller. The virtual resistance (r_L) is used for limiting the inner current. The filter capacitor (C_0) is used to reduce the ripple content in DC and maintains constant DC voltage. In the load, ten LEDs are connected in series. Each LED has 2.5 V minimum breakdown voltage and an internal equivalent series resistance of R_s. The PI controller generates the error voltage by monitoring present voltage using a potential divider circuit. The triggering pulses are generated using SR flip flop and duty cycle is varied to control the output voltage.

B. MODES OF OPERATION

In first mode, S_1 and S_2 are turned on. The LED load is isolated from the input source. The inductor voltage is same as the source voltage and the capacitor voltage appears across the load. In second mode, switch S_1 is still on and switch S_2 is turned off. The inductor current increases linearly and reaches the maximum value. In mode 3, both switches are turned off. The inductor energy is discharged through the capacitor and load. In mode 4, S_2 is turned on and the inductor current is maintained as constant.

D_A and D_B denotes the duty cycle of S_1 and S_2, R_0 represents the equivalent LED string resistance. In the mathematical design, a parasitic model was used to approximate the driver's practical model. V_{D1}, V_{D2} signifies the potential drop across diodes D_1, D_2 and r_{D1}, r_{D2}, r_{S1}, r_{S2} denotes the equivalent resistance of diodes D_1, D_2 and switches S_1, S_2. By applying ampere second balance equation to the converter, the inductor current (i_L) of the converter is

$$i_L = \frac{V_{LED}}{R_0 (1 - D_B)} \tag{1}$$

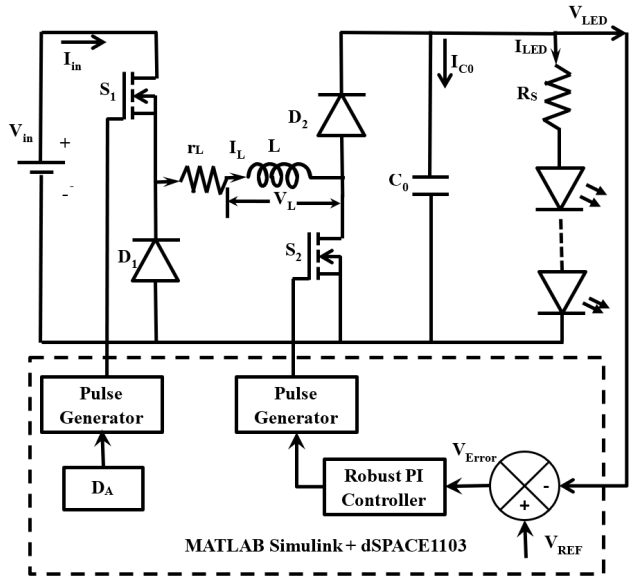

FIGURE 1. Circuit diagram of MHBC.

By applying voltage second balance equation to the converter, the LED voltage (V_{LED}) is

$$V_{LED} = \frac{R_0\,(1-D_B)\,\left(V_{in}D_A - V_{drop}\right)}{R_0\,(1-D_B)^2 + R_{drop}} \tag{2}$$

where,

$$V_{drop} = V_{D1}\,(1-D_A) + V_{D2}\,(1-D_B)$$
$$R_{drop} = r_{S1}D_A + r_{s2}D_B + r_{D1}\,(1-D_A) + r_{D2}\,(1-D_B) + r_L$$
$$\mathrm{T(S)} = \frac{\mathrm{V_{LED}}}{\mathrm{V_{in}}} = \frac{\mathrm{D_B'D_A/LC_0}}{\mathrm{s^2 + s\left(\frac{1}{C_0R_0} + \frac{R_{drop}}{L}\right) + \left(\frac{R_{drop} + (1-D_B)^2R_0}{LR_0C_0}\right)}} \tag{3}$$

Equation (3) is the open loop transfer function of the converter. It has no zeros and all poles are on the left half of the s plane. The system is stable for wide range of input variations with minimum phase.

C. SMALL SIGNAL CONTROLLER MODELLING

The small signal model is essential for controller design. The inductor current (i_L), output voltage (V_{LED}), duty cycle and input voltage (V_{in}) are considered as perturbed state variables in single loop voltage mode controller (SLVMC). The expressions for perturbations are, $x = X + \hat{x}$; $d = D + \hat{d}$; $u = U + \hat{u}$; $v_{LED} = V_{LED} + \hat{v}_{LED}$, where X, D, U, V_{LED} are steady state values and $\hat{x}$, $\hat{d}$, $\hat{u}$, $\hat{v}_{LED}$ are the perturbated values.

The state equations for different modes of operation with duty cycles are represented as follows:

$$\dot{x} = \dot{\hat{x}} = \Big[A_1(d_1+\hat{d}) + A_2(d_2+\hat{d}) + A_3(d_3+\hat{d}) + A_4(d_4+\hat{d})\Big]\,\hat{x} + \Big[B_1(d_1+\hat{d}) + B_2(d_2+\hat{d}) + B_3(d_3+\hat{d}) + B_4(d_4+\hat{d})\Big]\,u \tag{4}$$

$$\begin{bmatrix} \frac{d\hat{i}_L(t)}{dt} \\ \frac{d\hat{v}_{LED}(t)}{dt} \end{bmatrix} = A\hat{x} + \left(B_x\hat{d} + B_y\hat{V}_{in}\right) = \begin{bmatrix} 0 & \frac{-(1-D_B)}{L} \\ \frac{1-D_B}{C} & -\frac{1}{RC} \end{bmatrix} \times \begin{bmatrix} \hat{i}_L \\ \hat{v}_{LED} \end{bmatrix} + \begin{bmatrix} \frac{V_{LED}}{L} \\ \frac{i_L}{C} \end{bmatrix}\hat{d} + \begin{bmatrix} \frac{D_A}{L} \\ 0 \end{bmatrix}\hat{V}_{in} \tag{5}$$

$$\hat{i}_L = C_1\hat{x} = \begin{bmatrix} 1 & 0 \end{bmatrix}\begin{bmatrix} \hat{i}_L \\ \hat{v}_{LED} \end{bmatrix} \tag{6}$$

$$\hat{V}_{LED} = C_2\hat{x} = \begin{bmatrix} 0 & 1 \end{bmatrix}\begin{bmatrix} \hat{i}_L \\ \hat{v}_{LED} \end{bmatrix} \tag{7}$$

where,

$$A = \begin{bmatrix} 0 & \frac{-(1-D_B)}{L} \\ \frac{1-D_B}{C} & -\frac{1}{RC} \end{bmatrix};\quad B_x = \begin{bmatrix} \frac{V_{LED}}{L} \\ \frac{i_L}{C} \end{bmatrix};\quad B_y = \begin{bmatrix} \frac{D_A}{L} \\ 0 \end{bmatrix}$$
$$C_1 = \begin{bmatrix} 1 & 0 \end{bmatrix};\quad C_2 = \begin{bmatrix} 0 & 1 \end{bmatrix}$$

In this system, it is decided to control the duty cycle of switch S_2. The different dynamic transfer functions are derived from (5) – (7) such as duty cycle control to output voltage transfer function (G_A), input voltage to output voltage transfer function (G_B), duty cycle control to inductor current transfer function (G_C) and inductor current to output voltage transfer function (G_D).

$$G_A(s) = \frac{\hat{V}_{LED}(s)}{\hat{d}(s)} = C_2\,(SI - A)^{-1}\,B_1 = \frac{-s\left(\frac{I_L}{C_0}\right) + \frac{1}{LC_0}\left(V_{LED}\,(1-D_B) - R_{drop}I_L\right)}{s^2 + s\left(\frac{1}{C_0R_0} + \frac{R_{drop}}{L}\right) + \left(\frac{R_{drop} + (1-D_B)^2R_0}{LR_0C_0}\right)} \tag{8}$$

$$G_B(s) = \frac{\hat{V}_{LED}(s)}{\hat{V}_{in}(s)} = C_2\,(SI - A)^{-1}\,B_2 = \frac{\frac{(1-D_B)\,D_A}{LC_0}}{s^2 + s\left(\frac{1}{C_0R_0} + \frac{R_{drop}}{L}\right) + \left(\frac{R_{drop} + (1-D_B)^2R_0}{LR_0C_0}\right)} \tag{9}$$

$$G_C(s) = \frac{\hat{I}_L(s)}{\hat{d}(s)} = C_1\,(sI - A)\,B_1 = \frac{s\,\frac{V_{LED}}{L} + \frac{2V_{LED}}{LC_0R_0}}{s^2 + s\left(\frac{1}{C_0R_0} + \frac{R_{drop}}{L}\right) + \left(\frac{R_{drop} + (1-D_B)^2R_0}{LR_0C_0}\right)} \tag{10}$$

TABLE 1. Circuit parameters of MHBC.

Parameters	NOMINAL VALUE [10]	Variation [20]
Input DC voltage (V_{IN})	48 V	-80% +12%
MOSFET drain source resistance (r_{S1} & r_{S2})	0.077 Ω	±20%
Capacitor (C_0)	15 µF	±20%
Inductor (L)	1mH	±10%
Inductor ESR (r_L)	0.001Ω	-10%, +90%
Diode voltage drop (V_{D1} , V_{D2})	0.7V	±30%
Diode forward resistance (r_{D1} , r_{D2})	0.001 Ω	-10%, +50%
Output voltage (V_{LED})	30 V	
Switching frequency (f_{sw})	20 kHz	

$$G_D(s) = \frac{\hat{V}_{LED}(s)}{\hat{I}_L(s)} = \frac{G_A(s)}{G_C(s)} = \frac{-s\left(\frac{I_L L}{C_0 V_{LED}}\right) + \frac{1}{V_{LED} C_0}\left(V_{LED}(1-D_B) - R_{drop} I_L\right)}{s + \frac{2}{C_0 R_0}} \tag{11}$$

III. DYNAMICS OF A CONVERTER UNCERTAINTY

The Kharitonov's theorem which is the extension of Routh Hurtitz stability criterion is used to analyze the system with interval polynomial analysis. It helps in frequency analysis for guaranteed margin and PI controller stability region [19]

A. EFFECT OF PARAMETER UNCERTANITY

The dynamic behavior of the converter for input voltage is discussed. In addition, the parameter variations of the converter are considered for controller design under normal and abnormal conditions. The parameters nominal value are listed in Table 1. The input variation is based on usage of 48 V in EV applications [3], [4] and parameter variation is referred in robust control of DC to DC converter [20]. The converter performance is analyzed using different transfer functions as shown in Fig. 2. The duty cycle is varied to maintain constant load voltage for input and converter parameter variations. LED lighting is a sensitive load and it may fail whenever there is a sudden change in the driver parameters. Hence, variation in r_{S1}, r_{S2}, C_0, L, r_L, V_{D1}, V_{D2}, r_{D1}, r_{D2} and R_0 are considered. Based on the parameter variation in Table 1, the interval range for the transfer function coefficients are listed in Table 2.

The frequency domain analysis (bode plot) approach is used to analyze the relative stability of the system. The frequency response plots for various frequencies are shown in Fig. 3. In Fig. 3 (a), there is a non-minimum phase in which all poles and zeros lie in the left-hand side of s-plane. In Fig. 3 (b) and (c), there is a minimum phase and one zero lies on the right-hand side of s-plane which results in unstable system because of duty cycle variation. Hence, a negative integral gain value is required to compensate the zeros in the positive side which may result in stability issues. A proper design in zero compensator is required with stable and good transient response.

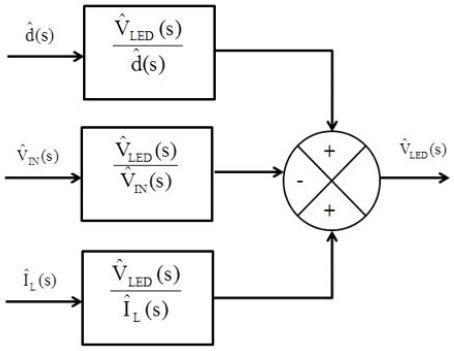

FIGURE 2. Dynamic model of MHBC.

TABLE 2. Circuit parameters coefficient range of MHBC.

Transfer function	Parameter uncertainty range
$\frac{\hat{V}_{LED}(s)}{\hat{d}(s)} = \frac{sb_{11}+b_{01}}{s^2+a_{11}s+a_{01}}$	$1.31\times10^9 < b_{01} < 2.44\times10^9$ $-4.42\times10^4 < b_{11} < -6.62\times10^4$ $3.92\times10^7 < a_{01} < 7.12\times10^7$ $1128 < a_{11} < 1651$
$\frac{\hat{V}_{LED}(s)}{\hat{V}_{IN}(s)} = \frac{b_{02}}{s^2+a_{12}s+a_{02}}$	$2.25\times10^7 < b_{02} < 4.48\times10^7$ $3.92\times10^7 < a_{12} < 7.18\times10^7$ $1128 < a_{12} < 1651$
$\frac{\hat{V}_{LED}(s)}{\hat{I}_L(s)} = \frac{sb_{13}+b_{03}}{s+a_{03}}$	$4.8\times10^4 < b_{03} < 7.3\times10^4$ $-1.62 < b_{13} < -2$ $2593 < a_{03} < 3889$

where,

$$b_{11} = -\left(\frac{I_L}{C_0}\right); \quad b_{01} = \frac{1}{LC_0}\left(V_{LED}(1-D_B) - R_{drop} I_L\right)$$

$$a_{11} = \frac{1}{C_0 R_0} + \frac{R_{drop}}{L}; \quad a_{01} = \frac{R_{drop} + (1-D_B)^2 R_0}{LR_0 C_0}$$

$$b_{02} = \frac{(1-D_B) D_A}{LC_0}$$

$$a_{12} = \frac{1}{C_0 R_0} + \frac{R_{drop}}{L}; \quad a_{02} = \frac{R_{drop} + (1-D_B)^2 R_0}{LR_0 C_0}$$

$$b_{13} = \frac{I_L L}{C_0 V_{LED}}; \quad b_{03} = \frac{1}{V_{LED} C_0}\left(V_{LED}(1-D_B) - R_{drop} I_L\right)$$

$$a_{03} = \frac{2}{C_0 R_0}$$

B. INTERVAL PLANT STABILIZATION KHARITONOV'S THEOREM

The Kharitonov's theorem is used for stability analysis and to identify boundary region of controller design. It generates

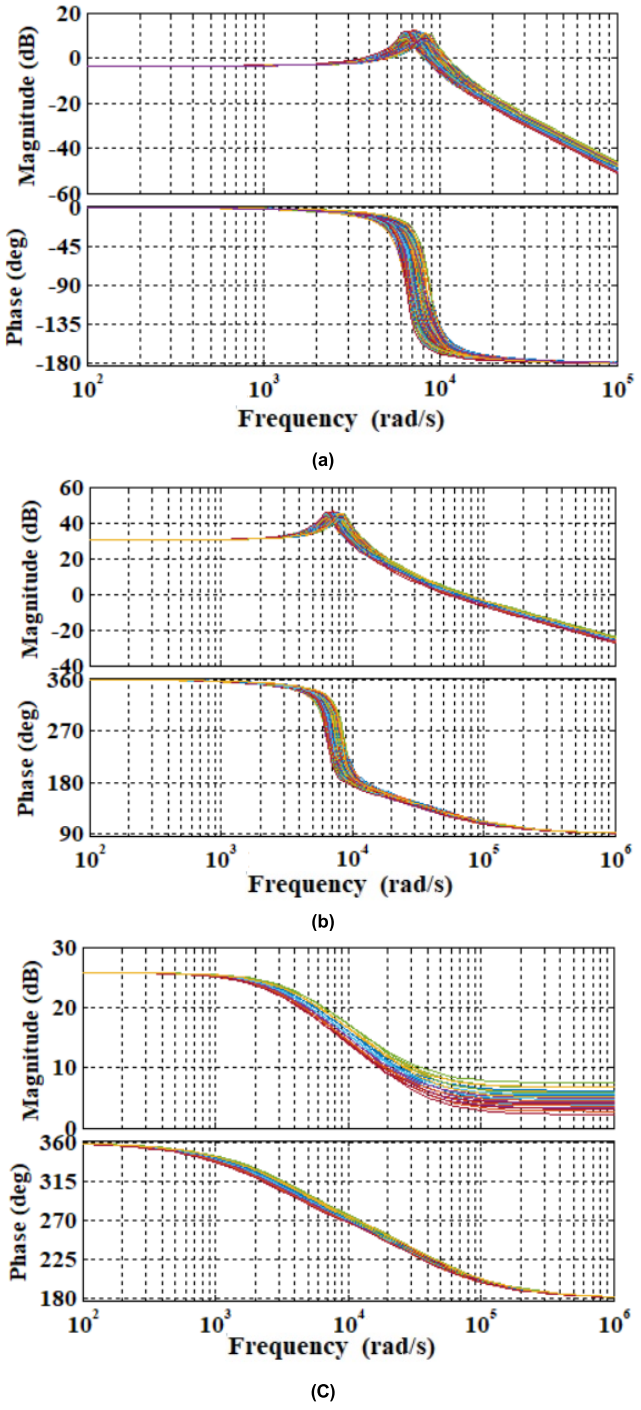

FIGURE 3. Bode plot with uncertainty parameters in the dynamic model (a) $\frac{\hat{v}_{LED}(s)}{\hat{v}_{IN}(s)}$ (b) $\frac{\hat{v}_{LED}(s)}{\hat{d}(s)}$ (c) $\frac{\hat{v}_{LED}(s)}{\hat{i}_{L}(s)}$.

different possible transfer functions with all possible combinations including the uncertainty range of system parameters. Hurwitz polynomial characteristic equation shows the stability information about the interval plant transfer function. Its polynomial range is between q_{nmin} and q_{nmax}, where n represents the order of the characteristic equation and q represents the minimum and maximum values of coefficient [18], [19].

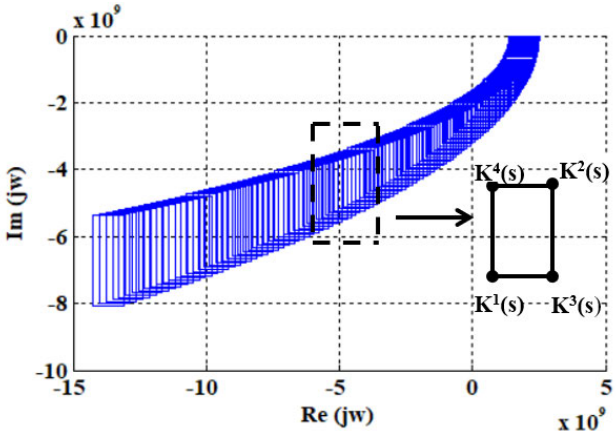

FIGURE 4. Kharitonov'S rectangles.

The polynomial Hurwitz characteristic equation is as follows:

$$P(s,q) = \sum_{i=0}^{n} q_i s^i; \quad where, \; q_{i\min} \le q_i \le q_{i\max} \tag{12}$$

$$P(s,q) = [q_{0\min}\; q_{0\max}] + [q_{1\min}\; q_{1\max}]\; s^1 + [q_{2\min}\; q_{2\max}]\; s^2 + \ldots\ldots + [q_{n\min}\; q_{n\max}]\; s^n \tag{13}$$

The polynomial equation is solved by Lyapunov's second method to reduce Hermite matrix of the four Kharitonov's polynomials (12) and create the Kharitonov's rectangular box. In this box, the stability of the interval plant is identified.

$$\begin{aligned}
K^1(s,q) &= q_{0\min} + q_{1\min}s + q_{2\max}s^2 + q_{3\max}s^3 + q_{4\min}s^4 + \ldots\ldots\ldots \\
K^2(s,q) &= q_{0\max} + q_{1\max}s + q_{2\min}s^2 + q_{3\min}s^3 + q_{4\max}s^4 + \ldots\ldots\ldots \\
K^3(s,q) &= q_{0\max} + q_{1\min}s + q_{2\max}s^2 + q_{3\min}s^3 + q_{4\max}s^4 + \ldots\ldots\ldots \\
K^4(s,q) &= q_{0\min} + q_{1\max}s + q_{2\min}s^2 + q_{3\max}s^3 + q_{4\min}s^4 + \ldots\ldots\ldots
\end{aligned} \tag{14}$$

The polynomial equations are developed based on the converter input variations and parameter uncertainty. The characteristic equation of single loop control with input and duty cycle variations for unity feedback system is given in (13) and the obtained Kharitonov's polynomials are presented in (14). The response of the system is analyzed for a maximum switching frequency of 20 kHz. The real and imaginary plot of Kharitonov's polynomials is rectangular in shape for variation in frequency as shown in Fig. 4. As all rectangles not encircles the origin point, Hurwitz polynomial is stable for all uncertainty condition with the boundary limit [21].

$$P(s) = 1 + G_A(s) = \left[(a_{01}+b_{01})_{\min}\,(a_{01}+b_{01})_{\max}\right] + \left[(a_{11}+b_{11})_{\min}\,(a_{11}+b_{11})_{\max}\right]\; s^1 + [11]\; s^2 \tag{15}$$

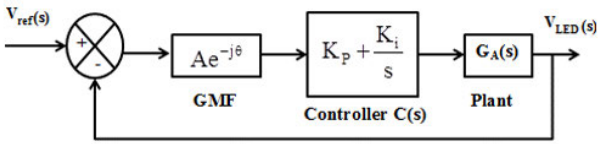

FIGURE 5. Plant controller with GMF.

$$K^1(s) = (a_{01} + b_{01})_{\min} + (a_{11} + b_{11})_{\min} s + s^2$$
$$K^2(s) = (a_{01} + b_{01})_{\max} + (a_{11} + b_{11})_{\max} s + s^2$$
$$K^3(s) = (a_{01} + b_{01})_{\max} + (a_{11} + b_{11})_{\min} s + s^2$$
$$K^4(s) = (a_{01} + b_{01})_{\min} + (a_{11} + b_{11})_{\max} s + s^2 \quad (16)$$

IV. ROBUST CONTROLLER DESIGN

A. GUARANTEED MARGIN FOR NOMINAL CONVERTER

The SLVMC should meet the required gain margin (GM) and phase margin (PM) with satisfied time domain specifications. Fig. 5 shows the MHBC SLVM with added guaranteed margin function (GMF) in (15) where A and θ represents the required gain margin and phase margin respectively. It is required to choose the marginal values for stability and robustness checking. Here, C(s) represents the PI controller transfer function and $G_A(s)$ represents the converter transfer function.

$$M(A, \theta) = Ae^{-j\theta} \quad (17)$$

The odd and even coefficients in the numerator and denominator components are segregated for obtaining Hurwitz polynomial which includes GMF and PI controller. Its polynomial characteristic equation is

$$P(s, M, C) = 1 + Ae^{-j\theta} C(s) G_A(s)$$
$$= 1 + (A\cos(\theta) - jA\sin(\theta)) \left(K_P + \frac{K_I}{s}\right) \left(\frac{N_A(s)}{D_A(s)}\right) \quad (18)$$

$$P(j\omega, M, C) = 1 + (A\cos(\theta) - jA\sin(\theta))$$
$$= \left(K_P + \frac{K_I}{j\omega}\right) \left(\frac{N_{AE}(-\omega^2) + j\omega N_{AO}(-\omega^2)}{D_{AE}(-\omega^2) + j\omega D_{AO}(-\omega^2)}\right) \quad (19)$$

The controller gain is obtained by segregating the real part and imaginary part and equating it to zero, (20) and (21), as shown at the bottom of the page.

The gain and phase margin of the system defines the relative stability and desired closed loop system transient response. As a result of different margins, various real root boundaries, complex root boundaries and infinite root boundaries are obtained. The stability region of the controller for various values of K_P and K_I based on the variation of ω is obtained. The selection of maximum frequency [20] is important to get proper finite region with condition $\mathrm{Im}(G_A(j\omega)) = 0$ and the maximum frequency is 1.6 kHz.

B. SELECTION OF CONTROLLER REGION WITH GMF

Fig. 6 shows the region for GMF to generate the PI gain and transient response. The values in the shaded region is fully stable and has minimum peak overshoot. The different gain margin with zero phase margin curve is shown in Fig. 6(a). The shaded region shows the guaranteed GM of $A = 1 \cap A = 2 \cup A = 3$ with stable points and minimum peak over shoot. The values of K_P and K_I obtained from the shaded area are $K_P = -0.015$ to 0.015 and $K_I = 0$ to 22. Based on this, the transient response for fixed gain margin and different phase margin is shown in Fig. 6(b). The shaded portion of the image depicts a stability area for nominal plants with $K_P = -0.015$ to 0.008 and $K_I = 0$ to 22.

C. SELECTION OF CONTROLLER REGION WITH SIXTEEN PLANT GMF

The Kharitonov's sixteen plant [18] is generated based on MHBC uncertain parameters. In a continuous time nonlinear system, the stability is analyzed for both normal and abnormal conditions. This approach is extended to robustness criteria for more number of possible uncertain combinations. The guaranteed margin controller gain derivations are obtained from plant (18)-(21) and those expressions are as follows, (22)–(24), as shown at the bottom of the next page, where N_A^{ij} *and* D_A^{ij} (i,j = 1,2,3,4) represents sixteen Kharitonov's nonlinear plant based on parameter uncertainty of numerator and denominator coefficients for multi linear interval systems.

Fig. 7(a)-(c) show the sixteen-plant frequency response gain and phase margin of the plant, nyquist plots and pole zero mapping. On account of the non-minimum system, single zero is in RHP. The entire poles in each plant is in LHP and it is nearer to origin plane when compared to zeros. All plants get negative gain and phase margin in open loop system for perturbations of input with respect to duty cycle. Hence, a superlative controller is required for all sixteen-plant

$$K_P = \frac{\sin(\theta)\ \omega \left[N_{AE}(-\omega^2) D_{AO}(-\omega^2) - N_{AO}(-\omega^2) D_{AE}(-\omega^2)\right] - \cos(\theta) \left[N_{AE}(-\omega^2) D_{AE}(-\omega^2) - \omega^2 N_{AO}(-\omega^2) D_{AO}(-\omega^2)\right]}{A\left[N_{AE}^2(-\omega^2) + \omega^2 N_{AO}^2(-\omega^2)\right]} \quad (20)$$

$$K_I = \frac{\sin(\theta)\ \omega \left[N_{AE}(-\omega^2) D_{AE}(-\omega^2) - \omega^2 N_{AO}(-\omega^2) D_{AO}(-\omega^2)\right] - \cos(\theta)\ \omega^2 \left[N_{AE}(-\omega^2) D_{AO}(-\omega^2) - N_{AO}(-\omega^2) D_{AE}(-\omega^2)\right]}{A\left[N_{AE}^2(-\omega^2) + \omega^2 N_{AO}^2(-\omega^2)\right]} \quad (21)$$

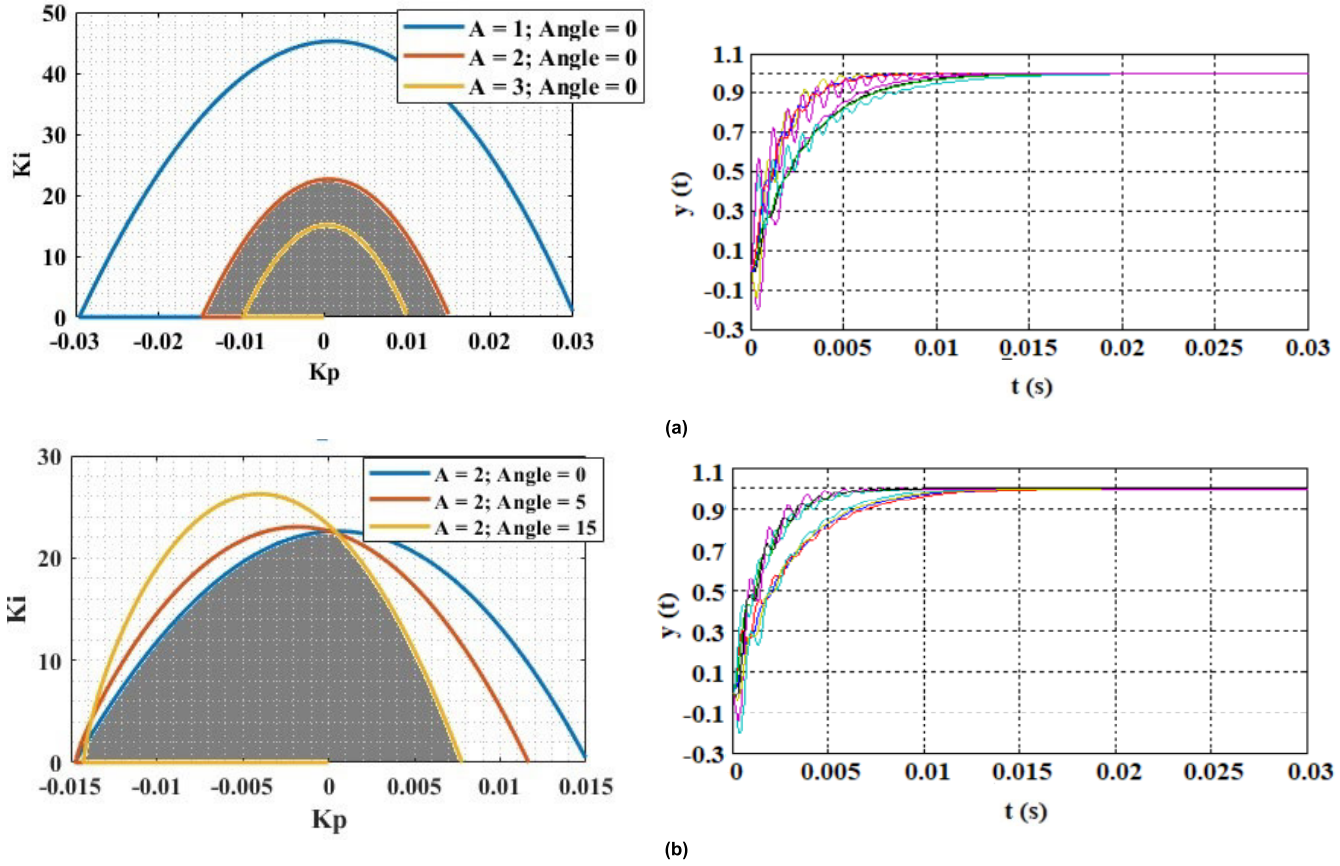

FIGURE 6. Stability region of nominal converter for different controller gains (a) Different gain margin and step response of the shaded region (b) Different phase margin and step response of the shaded region.

transfer function to make it a stable and for good transient response.

The variation in frequency and controller gain for sixteen plants is shown in Fig. 8. The controller gain values are intersection to all plants $\left(G_A^{11} \cap G_A^{12} \cap G_A^{13} \ldots\ldots\ldots\ldots \cap G_A^{44}\right)$. The values K_P and K_I correspond to the shaded area are $K_P = -0.015$ to 0.005 and $K_I = 0$ to 21except zero gain value. The range of controller gain without uncertain variations are $K_p = -0.015$ to 0.008 $K_i = 0$ to 22. The closed loop transfer function of the system for $K_P = 2e^{-3}$ and $K_I = 8$ is

$$G(s) = \frac{b_{24}\, s^2 + b_{14}\, s + b_{04}}{s^3 + a_{24}\, s^2 + a_{14}\, s + a_{04}} \tag{25}$$

$$\begin{aligned} \delta^{ij}(s) &= 1 + Ae^{-j\theta} C^{ij}(s)\, G_A^{ij}(s) \\ &= 1 + (A\ \cos\ (\theta) - jA\ \sin\ (\theta))\left(K_P^{ij} + \frac{K_I^{ij}}{s}\right)\left(\frac{N_A^{ij}(s)}{D_A^{ij}(s)}\right) \end{aligned} \tag{22}$$

$$K_P^{ij} = \frac{\begin{array}{l}\sin(\theta)\ \omega\ \left[N_{AE}^{ij}\left(-\omega^2\right) D_{AO}^{ij}\left(-\omega^2\right) - N_{AO}^{ij}\left(-\omega^2\right) D_{AE}^{ij}\left(-\omega^2\right)\right] \\ -\cos(\theta)\ \left[N_{AE}^{ij}\left(-\omega^2\right) D_{AE}^{ij}\left(-\omega^2\right) - \omega^2 N_{AO}^{ij}\left(-\omega^2\right) D_{AO}^{ij}\left(-\omega^2\right)\right]\end{array}}{A\left[N_{AE}^{ij}\left(-\omega^2\right)^2 + \omega^2 N_{AO}^{ij}\left(-\omega^2\right)^2\right]} \tag{23}$$

$$K_I^{ij} = \frac{\begin{array}{l}\sin(\theta)\ \omega\ \left[N_{AE}^{ij}\left(-\omega^2\right) D_{AE}^{ij}\left(-\omega^2\right) - \omega^2 N_{AO}^{ij}\left(-\omega^2\right) D_{AO}^{ij}\left(-\omega^2\right)\right] \\ -\cos(\theta)\,\omega^2\ \left[N_{AE}^{ij}\left(-\omega^2\right) D_{AO}^{ij}\left(-\omega^2\right) - N_{AO}^{ij}\left(-\omega^2\right) D_{AE}^{ij}\left(-\omega^2\right)\right]\end{array}}{A\left[N_{AE}^{ij}\left(-\omega^2\right)^2 + \omega^2 N_{AO}^{ij}\left(-\omega^2\right)^2\right]} \tag{24}$$

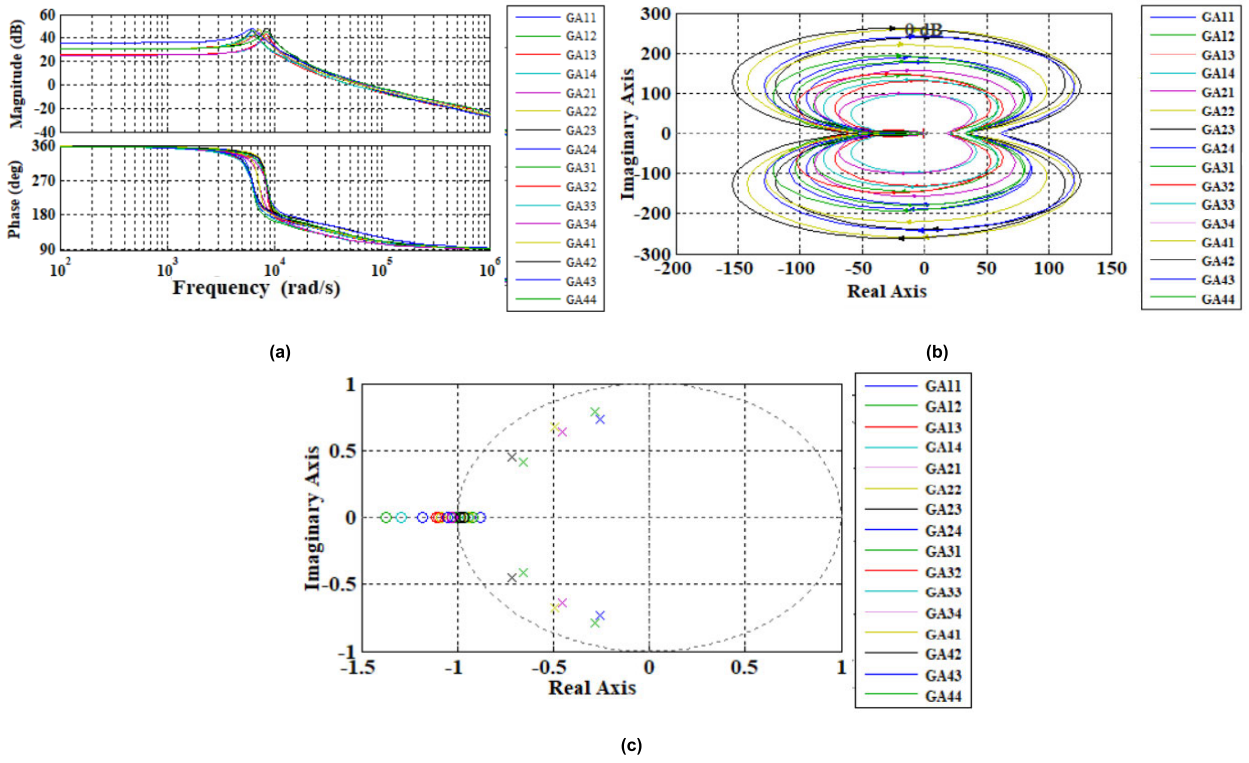

FIGURE 7. Sixteen Kharitonov's plants uncertainty in MHBC (a) Bode plot (b) Nyquist plot (c) Pole zero mapping.

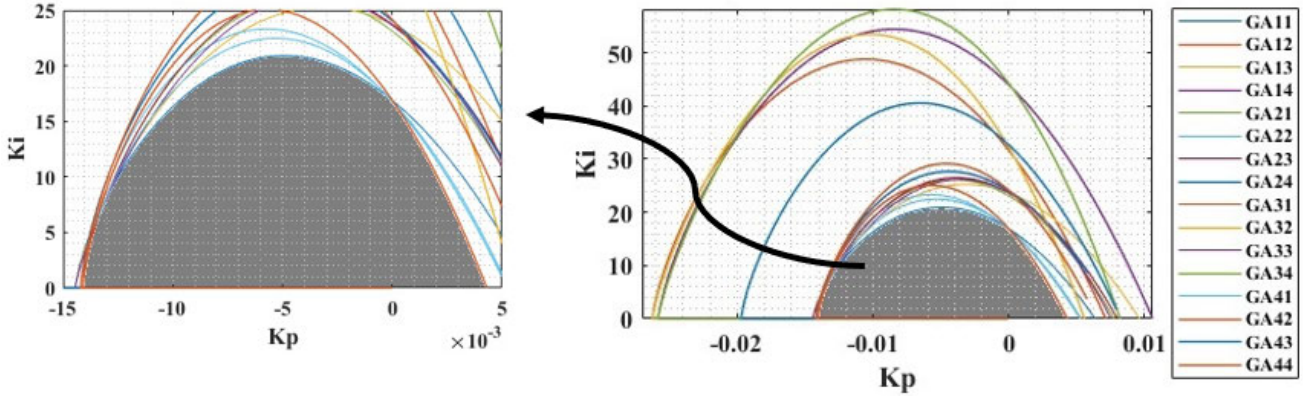

FIGURE 8. Stability region of robust PI controller GMF of sixteen Kharitonov's plant.

where,

$$\begin{aligned} -88.4 &\le b_{24} \le 133.2 \\ 2.3 \times 10^6 &\le b_{14} \le 4.5 \times 10^6 \\ 1.0 \times 10^{10} &\le b_{04} \le 1.9 \times 10^{10} \\ 994 &\le a_{24} \le 1563 \\ 4.1 \times 10^6 &\le a_{14} \le 7.5 \times 10^6 \\ 1.0 \times 10^{10} &\le a_{04} \le 1.9 \times 10^{10} \end{aligned}$$

D. DISCRETE TIME DOMAIN MODEL

The continuous time domain model of the system described in equation (25) is converted into discrete domain system using z transform. The system is sampled at sampling time period $T_s(ij) \gg 1/2\omega_{gc}(ij)$, where i, j are varied from one to four for various sixteen plant system. By considering the different values of controller gain in stability region, minimum value of ω_{gc} and maximum bandwidth is selected to achieve fast closed loop response. The discrete time domain transfer function for minimum T_s controller gain and sixteen plant discrete coefficient range is achieved using zero order hold and is expressed as

$$G(Z) = \frac{Z-1}{Z}\, Z\left(\frac{G(s)}{s}\right) \tag{26}$$

$$G(Z) = \frac{b_{25}Z^2 + b_{15}Z + b_{05}}{Z^3 + a_{25}Z^2 + a_{15}Z + a_{05}} \tag{27}$$

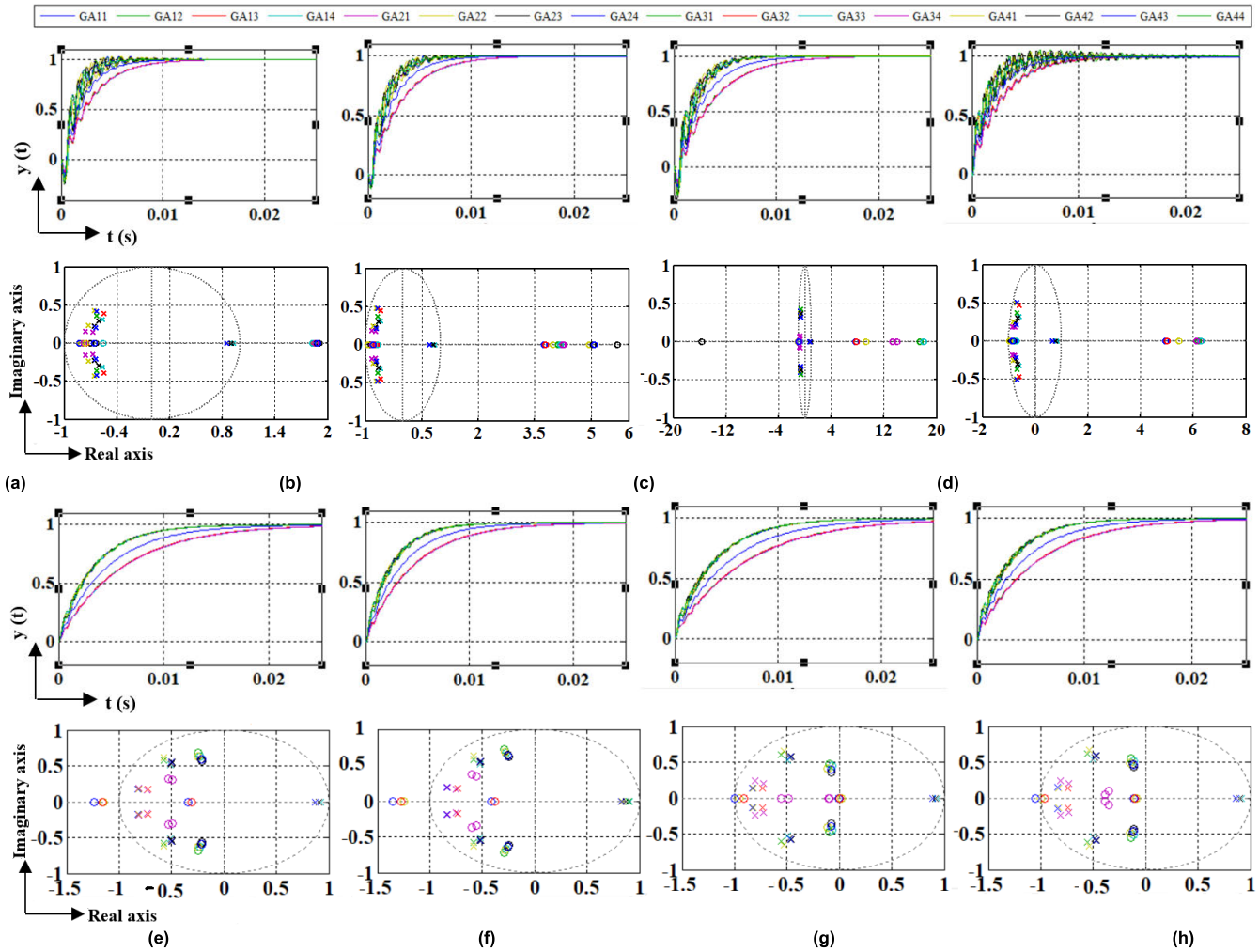

FIGURE 9. Step responses and pole zero map of sixteen Kharitonov's plants with gains (a) $K_P1 = -0.006$; $K_I1 = 8$ (b) $K_P2 = -0.006$; $K_I2 = 17$ (c) $K_P4 = -0.004$; $K_I4 = 16$ (d) $K_P6 = -0.006$; $K_I6 = 20$ (e) $K_P8 = 0.001$; $K_I8 = 9$ (f) $K_P9 = 0.001$; $K_I9 = 12$ (g) $K_P10 = 0.002$; $K_I10 = 8$ (h) $K_P11 = 0.002$; $K_I11 = 10$.

where,

$$0.13 \leq b_{25} \leq 0.2$$
$$0.03 \leq b_{15} \leq 0.18$$
$$0.01 \leq b_{05} \leq 0.04$$
$$0.1 \leq a_{25} \leq 0.7$$
$$-0.35 \leq a_{15} \leq -0.76$$
$$-0.49 \leq a_{05} \leq -0.63$$

E. PERFORMANCE ANALYSIS

In order to analysis the performance of the controller, the following random selection of controller gains are considered: The values of K_P and K_I are (a) $K_P1 = -0.006$ and $K_I1 = 8$ (b) $K_P2 = -0.006$ and $K_I2 = 17$ (c) $K_P4 = -0.004$ and $K_I4 = 16$ (d) $K_P6 = -0.006$ and $K_I6 = 20$ (e) $K_P8 = 0.001$ and $K_I8 = 9$ (f) $K_P9 = 0.001$ and $K_I9 = 12$ (g) $K_P10 = 0.002$ and $K_I10 = 8$ (h) $K_P11 = 0.002$ and $K_I11 = 10$. The step response of pole zero mapping for discrete model sixteen Kharitonov's plant values are shown in Fig. 9. Fig. 9 (a)-(d) have negative proportional gain and positive integral gain values and Fig. 9 (e)-(h) have a positive proportional gain and integral gain values. The step response of sixteen-plant system possesses minimum peak overshoot, faster rise and settling time. It is inferred from the pole zero mapping (PZM) plot that some of the zeros lie outside the unit circle for different controller gain. Hence, PZM with $K_P = 2e^{-3}$ and $K_I = 8$ is selected for practical validation as all poles and zeros are located inside the unit circle as in Fig. 9(g).

The step response of the nominal plant within stabilizing gain region is shown in Fig. 10 (a). It is noted that all responses get the minimum overshoot and smooth response at all operating conditions. The step response for variation in the input voltage with positive integrator gain

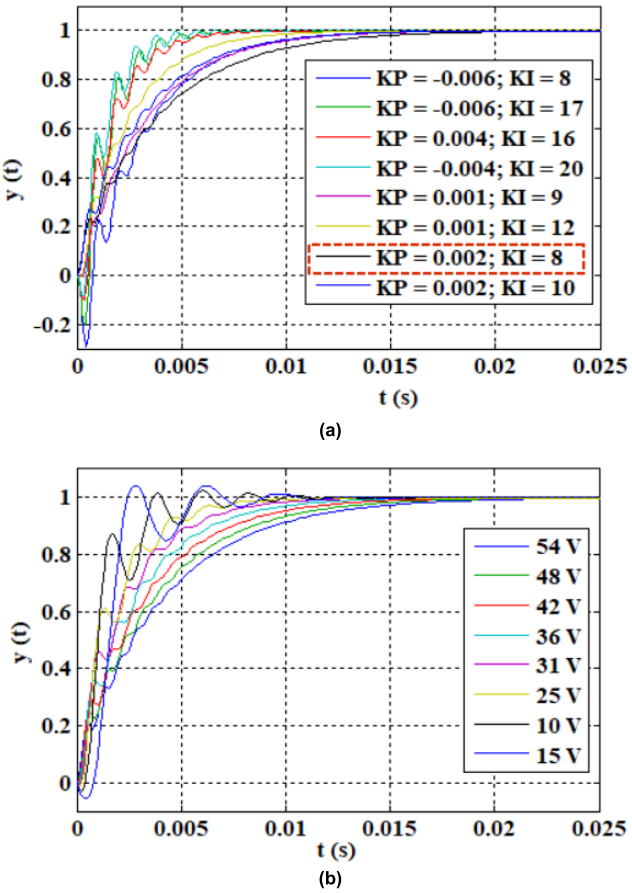

FIGURE 10. Step response of (a) nominal plant within stabilizing gain region (b) variation in input voltage with $K_P = 0.002$ and $K_I = 8$.

($K_P = 2e^{-3}$; $K_I = 8$) is shown in Fig. 10 (b). It is inferred that the controller works for wide input variations in MHBC.

F. CONTROLLER DESIGN PROCEDURE

Design procedure for single loop voltage mode robust controller are:

1) Obtain s domain continuous time transfer function using (8).
2) Select minimum and maximum values for uncertain parameters as represented in Table 1.
3) Calculate minimum and maximum values of coefficient of the controller as represented based on Table 2.
4) Using Kharitonov's rectangular theorem, check plant interval stability (16).
5) Plot controller gain (20) and (21) stability region using different GM and zero PM angle for the selected guaranteed GM.
6) Use selected GM and vary the PM to plot the controller's gain stability region as shown in Fig. 6 (b) for identifying the final nominal control plant robust stability region.

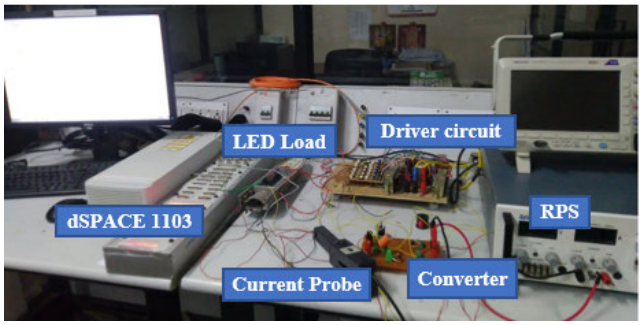

FIGURE 11. Experimental setup.

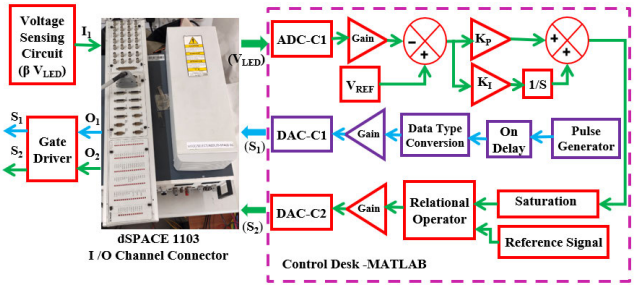

FIGURE 12. Schematic diagram of control scheme implementation of MHBC using dSPACE setup.

7) Based on selected guaranteed GM & PM, obtain Kharitonov's sixteen plant controller gain in (23) and (24). Plot all plant controller gains and obtain final uncertainty robust stability region as in the shaded region in Fig. 8.
8) Find the time domain performance index and validate the pole zero mapping using different controller parameters from the final stability region.
9) For the nominal plant, check the time domain index as in Fig. 10, for different controller gains. Also, check voltage uncertainty for the fixed controller gain values.

V. SIMULATION AND EXPERIMENTAL RESULTS

The simulation of closed loop system is performed in PSIM software as per the design specification in Table 1. To evaluate the performance of the developed controller, the gains $K_P = 1e^{-3}$ and $K_I = 8$ are chosen and the system is tested with input voltage variations of 15 V to 54 V. Similarly, prototype is developed using dSPACE1103 controller with MATLAB software interface.

A. EXPERIMENTAL SETUP

The converter is made up of two IRF540 MOSFET switches and two LT6A02 diodes. The control pulses are generated by DAC pin 1 in dspace controller with sampling frequency of 200 kHz and driven by TLP250 driver IC. The experimental setup of the system is shown in Fig. 11. SIGLENT CP4060 current probe is used to measure the current and

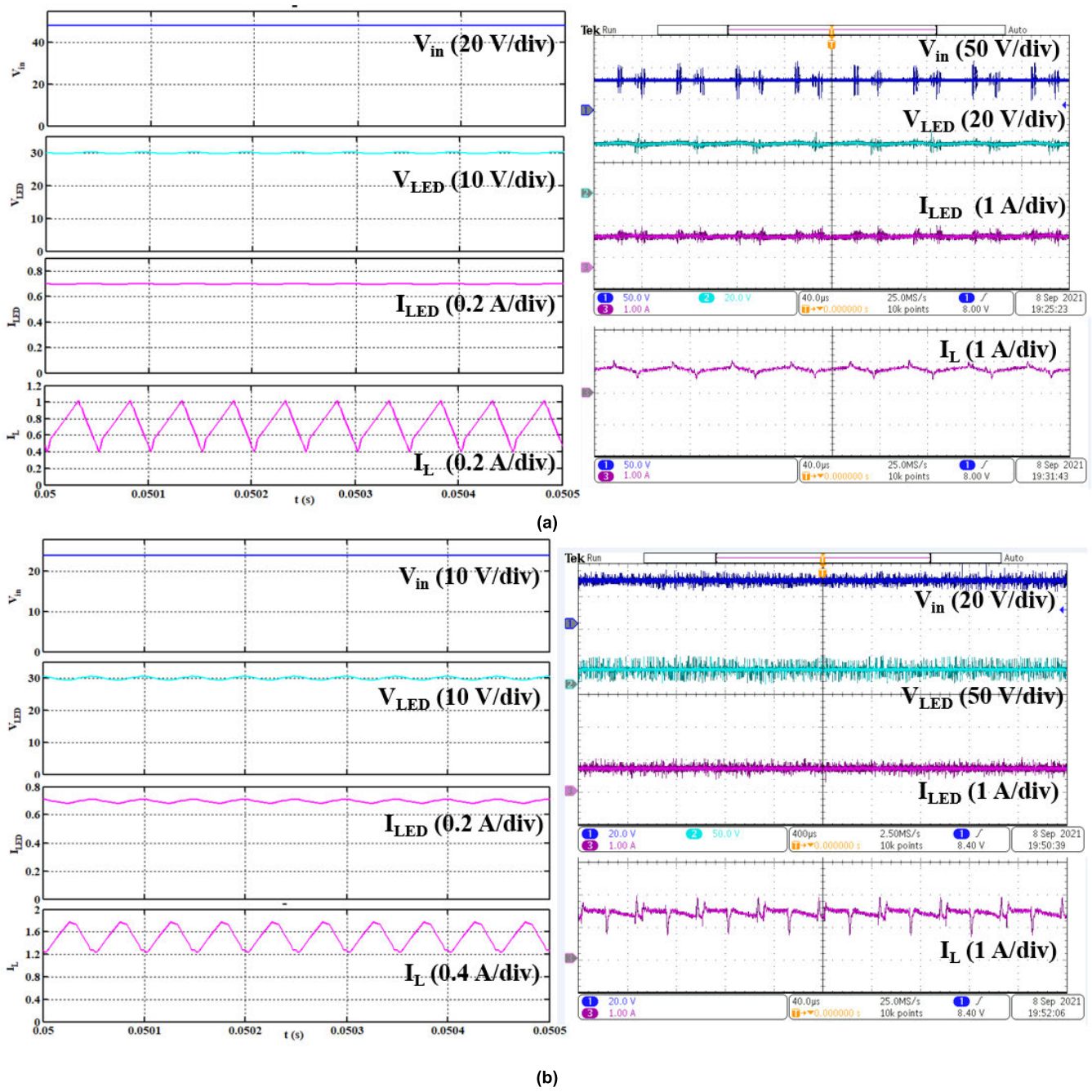

FIGURE 13. Simulation and experimental results of LED output voltage, LED output current and Inductor current of (a) 48 V input (b) 24 V input.

MDO3024 mixed domain oscilloscope is used to record the waveforms.

The control scheme implementation is shown in Fig. 12. Switch S_1 is controlled with fixed 55% duty cycle. The switching pulse for S_2 is generated from the controller to maintain constant output voltage for variations in input voltage. A potential divider is used to measure the output voltage and fed as input to ADC pin 1. To maintain a steady output voltage, the robust PI controller creates control pulses based on the error signal and feeds them as input to the driver circuit through DAC pin 2.

B. STEADY STATE AND DYNAMIC RESPONSE

The converter with SLVM controller is tested in both simulation and hardware for steady state input voltage of 48 V and 24 V as represented in Fig. 13. It shows the input voltage, output voltage, output current and inductor current of LED driver. Fig. 13 (a) shows the steady state input voltage

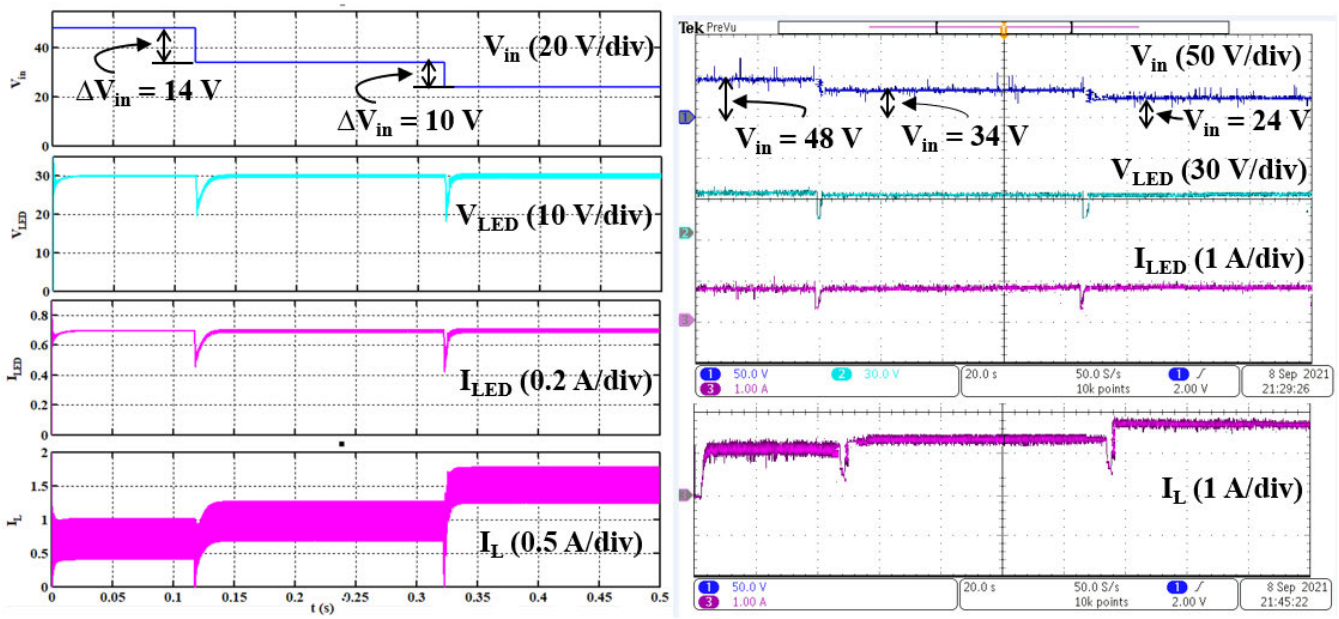

FIGURE 14. Simulation and experimental results of LED output voltage, LED output current and Inductor current of input dynamic variations.

TABLE 3. Different controller performance parameters.

Method of controller	Controller Gain	ISE ($\times 10^{-3}$)	GM (dB)	PM (degree)	t_r (ms)	t_s (ms)	M_p (%)
Proposed	$K_P = 2\times10^{-3}$; $K_I = 8$.	1.75	14.2	93	8	14	0
ZNF	$K_P = 12\times10^{-3}$; $K_I = 24.68$.	0.58	2.58	8.58	1	15	9.46
AMIG	$K_P = 0.46\times10^{-3}$; $K_I = 42.35$.	0.58	0.54	85.5	1	49	17.3
RRT	$K_P = 0$; $K_I = 6.17$.	2.42	17.3	89.3	10	14	0

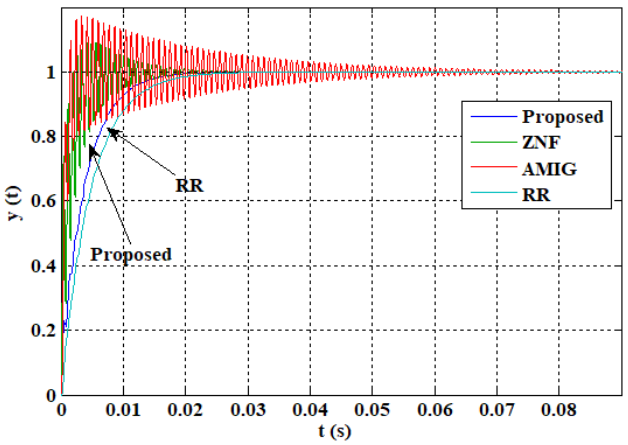

FIGURE 15. Step response of the converter with different controllers.

at 48 V to get 30 V output voltage and 700 mA output current. The LED output voltage and output current ripple is minimum in simulation and experimental results. The MHBC

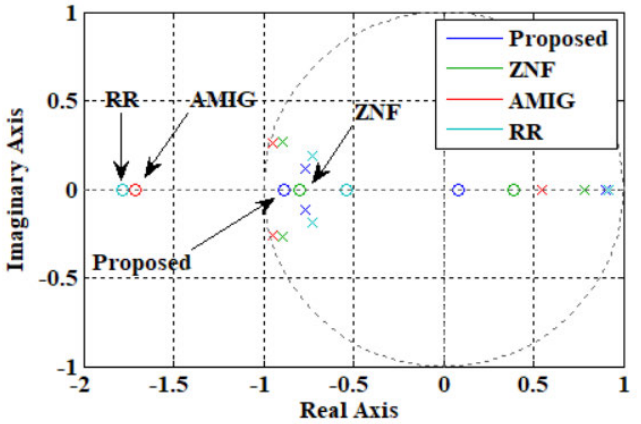

FIGURE 16. Pole- zero map of different controller.

is operated in continuous conduction mode and the inductor current is varying between 500 mA and 1 A. Similarly, input voltage, output voltage, output current and inductor current for 24 V are shown in Fig. 13(b). It is inferred that, there is some ripple in the inductor current and output current, since input voltage is reduced from 48 V to 24 V.

The simulation and experimental waveforms for dynamic response of the MHBC for variations in input voltage (ΔV_{in}) of 48 V, 34 V and 24 V are shown in Fig. 14. In simulation, the input voltage is varied at t = 0.12 s and t = 0.325 s. As a result of the non-minimum phase of the converter, there is a negative dip in all waveforms during dynamic variations and maintained constant after short duration. The corresponding input voltage, output voltage, output current and inductor current are shown in Fig. 14.

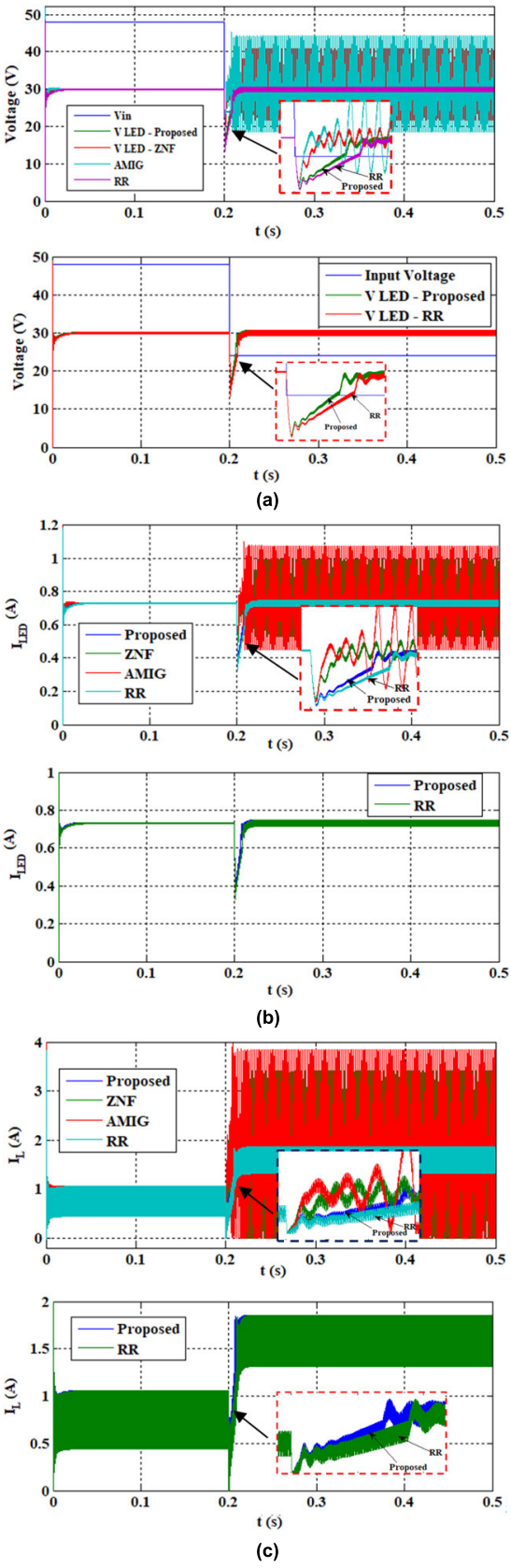

FIGURE 17. Simulation results for transient response of proposed and RR controller (a) output voltage (b) output current (c) inductor current.

C. PERFORMANCE COMPARISONS

The conventional PID controller is tuned using PID tuner app in MATLAB - SISO tool [22]. For turning the values of controller gains, various methods say Ziegler – Nicholos frequency response (ZNF), approximate MIGO frequency response (AMIG), robust response time (RR) are available. Fig. 15 shows the step response of the different controller and it is observed that proposed controller model gives fast response and zero peak overshoot. The pole zero mapping plane is shown in Fig. 16 and it is inferred that in the proposed controller, all pole zero mapping lies inside the unit circle In ZNF controller, though all poles and zeros lie inside unit circle, the system has more oscillations and slow response.

The peak value of sensitivity is represented as $M_s = \max_\omega \left| \frac{1}{1+G_A(j\omega)C(j\omega)} \right|$ in the characterization of performance and robustness of the feedback system. The peak sensitivity value is 1.34 in more aggressive robust controller [22]. It is inferred from Table 3 that RRT controller response is closer to the proposed controller but with only integral gain. Hence, it is difficult to process the instant data which creates lagging in the robustness.

The performance comparison of RR, ZNF, AMIG and proposed controller for MHBC is illustrated in Fig. 16. It is inferred that, ZNF and AMIG controllers have high peak overshoot, slow response and high steady state error. The RR controller possesses better response compared to ZNF and AMIG controller. Because of the absence of proposal gain in RR controller, the system possesses slow response compared with proposed controller. The simulation results for transient response for various controllers are shown in Fig. 17. The input voltage is varied from 48 V to 24 V at 0.2 s. The proposed controller has fast response with fast settling time. The corresponding load and inductor currents are illustrated in Fig. 17(b) and Fig. 17(c) respectively.

VI. CONCLUSION

This paper presents a robust controller fed MHBC for automotive LED lighting applications. A SLVMC is proposed for parametric variations in input voltage, equivalent drain source resistance of switches, output capacitance, inductance, inductor ESR, diode voltage drop, diode forward resistance and load resistance under uncertain conditions. As control is deployed on single switch, it reduces the control complexity. The controller compensates RHP zero by using guaranteed margin Kharitonov's theorem. The interval plant system stability is verified by Kharitonov's rectangular box. The controller design is discussed in systematic manner with analytical pathway for non-minimum phase DC-DC converter for improved dynamic response. The stability region is generated upon guaranteed gain and phase margin of the system for normal and abnormal conditions. For stability region, the abnormal condition's guaranteed gain and phase margin is considered. The system possesses better time domain spec-

ifications for $K_P = 2e^{-3}$ and $K_I = 8$ for the change in input voltage ranging from 15 V to 54 V. The performance improvement is achieved compared with different conventional PID controller tuning techniques. The proposed controller compensates the RHP zeros with 14 ms settling time, ISE as $1.75e^{-3}$ and peak sensitivity of 1.34. The detailed mathematical model is obtained for the system and tested in both simulation and experimental setup. The proposed robust controller design technique can be extended to any nonminimum phase DC to DC converter.

REFERENCES

[1] Y. Wang, J. M. Alonso, and X. Ruan, "A review of LED drivers and related technologies," *IEEE Trans. Ind. Electron.*, vol. 64, no. 7, pp. 5754–5765, Jul. 2017, doi: 10.1109/TIE.2017.2677335.
[2] X. Long, J. He, J. Zhou, L. Fang, X. Zhou, F. Ren, and T. Xu, "A review on light-emitting diode based automotive headlamps," *Renew. Sustain. Energy Rev.*, vol. 41, pp. 29–41, Jan. 2015, doi: 10.1016/j.rser.2014.08.028.
[3] K. Jost, "Application of 48 volt for mild hybrid vehicles and high power loads," in *48-Volt Developments*. Warrendale, PA, USA: SAE, 2016, ch. 7, pp. 93–104.
[4] L. K. Walker, "Battery test manual for 48 volt mild hybrid electric vehicles," Idaho Nat. Lab., Idaho Falls, ID, USA, Tech. Rep. NL/EXT-15-36567, 2017, doi: 10.2172/1389182.
[5] V. Harikrishna, R. Gunabalan, and S. S. Kumar, "Pulse width modulation converter for light-emitting diode tube light applications," *Int. Trans. Electr. Energy Syst.*, vol. 30, no. 4, pp. 1–10, Apr. 2020.
[6] A. Malschitzky, F. Albuquerque, E. Agostini, and C. B. Nascimento, "Single-stage integrated bridgeless-boost nonresonant half-bridge converter for LED driver applications," *IEEE Trans. Ind. Electron.*, vol. 65, no. 5, pp. 3866–3878, May 2018.
[7] S. Mukherjee, V. Yousefzadeh, A. Sepahvand, M. Doshi, and D. Maksimovic, "A two-stage automotive LED driver with multiple outputs," *IEEE Trans. Power Electron.*, vol. 36, no. 12, pp. 14175–14186, Dec. 2021.
[8] Y. Qin, S. Li, and S. Y. Hui, "Topology-transition control for wide-input-voltage-range efficiency improvement and fast current regulation in automotive LED applications," *IEEE Trans. Ind. Electron.*, vol. 64, no. 7, pp. 5883–5893, Jul. 2017.
[9] V. K. S. Veeramallu, S. Porpandiselvi, and B. L. Narasimharaju, "A non-isolated wide input series resonant converter for automotive LED lighting system," *IEEE Trans. Power Electron.*, vol. 36, no. 5, pp. 5686–5699, May 2021.
[10] A. Sureshkumar and R. Gunabalan, "Design and implementation of single switch control DC-DC converter with wide input variation in automotive LED lighting," *Int. Trans. Electr. Energy Syst.*, vol. 31, no. 4, pp. 1–22, 2021.
[11] R. W. Erickson and D. Maksimović, "Steady-state equivalent circuit modeling, losses, and efficiency," in *Fundamentals of Power Electronics*, vol. 6, 2nd ed. Amsterdam, The Netherlands: Kluwer, 2004, pp. 294–300.
[12] M. G. Kim, "High-performance current-mode-controller design of buck LED driver with slope compensation," *IEEE Trans. Power Electron.*, vol. 33, no. 1, pp. 641–649, Jan. 2018.
[13] Y. Zhang, J. Liu, Z. Dong, H. Wang, and Y.-F. Liu, "Dynamic performance improvement of diode–capacitor-based high step-up DC–DC converter through right-half-plane zero elimination," *IEEE Trans. Power Electron.*, vol. 32, no. 8, pp. 6532–6543, Aug. 2017.
[14] M.-F. Hung and K.-H. Tseng, "Study on the corresponding relationship between dynamics system and system structural configurations—Develop a universal analysis method for eliminating the RHP-zeros of system," *IEEE Trans. Ind. Electron.*, vol. 65, no. 7, pp. 5774–5784, Jul. 2018.
[15] N. Rana, A. Ghosh, and S. Banerjee, "Development of an improved tristate buck–boost converter with optimized type-3 controller," *IEEE J. Emerg. Sel. Topics Power Electron.*, vol. 6, no. 1, pp. 400–415, Mar. 2018.
[16] T. Kobaku, R. Jeyasenthil, S. Sahoo, and T. Dragicevic, "Experimental verification of robust PID controller under feedforward framework for a nonminimum phase DC–DC boost converter," *IEEE J. Emerg. Sel. Topics Power Electron.*, vol. 9, no. 3, pp. 3373–3383, Jun. 2021.
[17] J. Zhang and L. Guo, "Theory and design of PID controller for nonlinear uncertain systems," *IEEE Control Syst. Lett.*, vol. 3, no. 3, pp. 643–648, Jul. 2019.
[18] S. P. Bhattacharyya, "Robust control under parametric uncertainty: An overview and recent results," *Annu. Rev. Control*, vol. 44, pp. 45–77, 2017.
[19] R. Matušu, B. Senol, and L. Pekař, "Robust PI control of interval plants with gain and phase margin specifications: Application to a continuous stirred tank reactor," *IEEE Access*, vol. 8, pp. 145372–145380, 2020.
[20] F. Asadi and J. Hudgins, *Robust Control of DC-DC Converters: The Kharitonov's Theorem Approach With MATLAB Codes*. San Rafael, CA, USA: Morgan & Claypool, 2018.
[21] S. P. Bhattacharyya, A. Datta, and L. H. Keel, *Linear Control Theory: Structure, Robustness, and Optimization*. Boca Raton, FL, USA: CRC Press, 2009.
[22] M. Veerachary and N. Kumar, "Analysis and design of quadratic following boost converter," *IEEE Trans. Ind. Appl.*, vol. 56, no. 6, pp. 6657–6673, Nov./Dec. 2020.

ALAGARSAMY SURESHKUMAR received the B.E. degree in electrical and electronics engineering from Bharathiar University, Coimbatore, India, in 2004, and the M.E. degree in power electronics and drives from Anna University, Chennai, Tamil Nadu, India, in 2007. He is currently pursuing the Ph.D. degree with the School of Electrical Engineering, Vellore Institute of Technology, Chennai. His research interests include dc–dc power converters and robust controller design.

RAMACHANDIRAN GUNABALAN (Member, IEEE) received the B.E. degree in electrical and electronics engineering from Manonmanium Sundaranar University, Tirunelveli, Tamil Nadu, India, in 2000, the M.Tech. degree in electrical drives and control from Pondicherry University, in 2006, and the Ph.D. degree from Anna University, Chennai, Tamil Nadu, India, in 2015. He is an Associate Professor with the School of Electrical Engineering, Vellore Institute of Technology, Chennai. He has published 25 research articles in reputed journals and presented around 25 papers in national and international conferences. His research interests include dc–dc power converters and estimation and control of induction motor drives. He is a Life Member of ISTE and IEI.